Slab Ocean Component of the Exascale Earth System Model (E3SM): Development, Evaluation and Application to Understanding Earth System Sensitivity

Oluwayemi Garuba[1], Philip J. Rasch[1], L. Ruby Leung[1], Hailong Wang[1], Samson Hagos[1], Balwinder Singh[1]

[1]Pacific NorthWest National Laboratory

Key Points:

- Slab ocean model implementation in E3SMv2 is able to reproduce the model's baseline climate and equilibrium climate sensitivity very well.
- E3SMv2 Slab model experiments show a large surface temperature sensitivity to ocean heat transports, particularly in the Southern hemisphere.
- Temperature sensitivity to ocean heat transports are enhanced by the shortwave cloud radiative effect due to marine low-level cloud changes.

Corresponding author: Oluwayemi Garuba, `Oluwayemi.garuba@pnnl.gov`

Abstract

This work describes the implementation and evaluation of the Slab Ocean Model component of the Energy Exascale Earth System Model version 2 (E3SMv2-SOM), and its application to understanding the climate sensitivity to ocean heat transport (OHT) strength and CO_2 forcing. E3SMv2-SOM reproduces the baseline climate and Equilibrium Climate Sensitivity (ECS) of the E3SMv2 fully coupled experiments, reasonably well, with a pattern correlation close to 1 and global mean bias that is less than 1% of the fully coupled surface temperature, precipitation and sea ice extent and volume. Similar to other model behaviour, the ECS estimated from the SOM (4.5°C) is greater than the estimate from fully coupled model (4.0°C; from 150 years regression). The E3SMv2 baseline climate is also very sensitive to the strength of the OHT from which the prescribed ocean heat convergence (OHC) for the SOM is derived, with a surface temperature difference of about 4.0°C between high- and low-OHT SOM experiments. The surface temperature response in the high/low-OHT experiments occur through a positive/negative Shortwave cloud radiative effect, caused by a decrease/increase in marine low-level clouds over subpolar regions. This surface temperature sensitivity to prescribed OHCs is particularly large in the Southern hemisphere and is associated with an overcompensation of between prescribed OHC/OHT by atmosphere heat transports. This large sensitivity indicates stronger low-level cloud feedbacks in E3SM. The SOM's ECS estimate is also sensitive to the baseline climate it is initialized from, with an ECS difference of 0.5°C between the high- and low- OHT CO_2 increase experiments.

Plain Language Summary

The implementation and evaluation of the Slab Ocean Model (SOM) in the Exascale Earth System Model version 2 (E3SMv2) is described in this study. The SOM is evaluated by comparing its climate simulation to that of the full version of the model that uses a dynamic ocean model instead of a SOM. The SOM reproduces the baseline climate of the full E3SMv2, as well as the equilibrium surface global temperature response to CO_2 doubling of the full model reasonably well. The SOM is further used to test the sensitivity of the E3SM model to various ocean heat transport strengths. The results show that E3SMv2 has a large surface temperature sensitivity to ocean heat transport changes, particularly over the Southern Ocean. This large sensitivity occurs as a result of changes in marine low-level clouds, which cause changes in the shortwave radiation that reach the surface and enhance the surface temperature changes. Atmosphere heat transport also respond to and compensate ocean heat transport changes, and as a result of the large temperature response in the Southern Ocean, this compensation is also greater there. We also find that Ocean heat transport increases also reduce the equilibrium surface temperature response to CO_2 doubling.

1 Introduction

Slab Ocean models (SOM) are very useful tools for hierarchical ocean model studies and evaluation of climate sensitivity (Danabasoglu & Gent, 2009; Bitz et al., 2012; Jeevanjee et al., 2017; Dunne et al., 2020). A slab ocean model is a single layer approximation of a dynamic ocean model that is thermally coupled with the atmosphere and sea ice models. In contrast to a dynamic ocean model where circulation features (currents, transports, mixed layer depth, etc) are simulated and can evolve and change from year to year, the mixed layer thickness and net impact of ocean heat transports are prescribed for slab ocean models. As a result, the SOM is able to simulate the evolution of the ocean surface temperature and upper ocean heat content reasonably well, and is able to equilibrate very quickly to provide information at a fraction of the cost of a climate model with explicit ocean and sea ice dynamics.

While other configurations of Ocean Mixed Layer Models (MLM) have been used (e.g., Codron, 2012; Hirons et al., 2015; Hsu et al., 2022), the SOM configuration is more widely used because of its simplicity and ability to reproduce a model's climatology and climate sensitivity. The SOM configuration is different from these other ocean mixed layer model configurations because it doesn not include an explicit representation of ocean vertical mixing processes and surface wind changes on the ocean mixed layer. The SOM configuration, instead represents the net climatological impact of all ocean heat transport processes (including vertical mixing and advective processes) through the monthly climatological ocean heat convergence that is prescribed for the model.

Despite its usefulness, the SOM capability has not been implemented and evaluated in the Exascale Earth System model (E3SM). E3SM is a relatively new coupled model developed by the US Department of Energy (DOE) (Leung et al., 2020). The E3SM project (http://e3sm.org) aims to tackle the challenges important to DOE's mission to simulate and predict long term changes in environmental variables relevant for the US energy sector. The E3SM was branched from a variant of the Community Earth System Model (CESM) but has undergone significant changes. The atmospheric component uses the spectral element dynamical core instead of the finite volume grid (Rasch et al., 2019) and the Model for Prediction Across Scales (MPAS) framework is adopted for its Ocean and Sea ice component models (Ringler et al., 2013; Petersen et al., 2019), replacing CESM's choices for an ocean model. Here, we implement the "NEWSOM" formulation described in Bitz et al. (2012) into E3SM version 2 (E3SMv2) (Golaz et al., 2022). This SOM formulation was designed to reproduce the climatology of a fully coupled model, unlike earlier formulations of SOM that aim to reproduce observations (McFarlane et al., 1992; Kiehl et al., 2006; Schmidt et al., 2006; Knutson, 2003). The "NEWSOM" has an advantage of simulating realistic model sea ice climatology without requiring additional adjustments to the prescribed ocean heat convergence.

In section 2, we describe the SOM formulation in E3SMv2 and the sets of E3SMv2-SOM experiments that are used to evaluate and test its sensitivity to ocean heat transports. In the results section 3.1, the ability of SOM to reproduce the climatology of the fully coupled E3SMv2 pre-industrial control integration and its climate sensitivity to CO2 forcing is demonstrated. In section 3.2, the sensitivity of the E3SMv2 to variations in prescribed ocean heat convergence forcings, particularly for the relatively weak (compared to observational estimated) ocean heat transports from the E3SMv1/v2 low-resolution experiments and the stronger ocean heat transports produced in E3SMv1 high resolution and CESM simulations. We demonstrate that the SOM can indeed be a useful part of the E3SM capability suite.

2 Model description and experiments

This study is based on assessing a series of simulations in which the standard ocean model component in the Exascale Earth System Model versions 2 (E3SMv2, Golaz et al., 2022) is replaced with a SOM. The standard fully coupled E3SMv2 model contains the E3SM Atmosphere Model (EAM) (Rasch et al., 2019), the E3SM Land Model (ELM), Model for Prediction across scales MPAS ocean model (MPAS-O) and MPAS sea ice models (MPAS-SI) (Petersen et al., 2019) respectively. The E3SMv2-SOM configuration (E3SMv2-SOM) thus replaces the dynamic MPAS-O model component with the SOM component. While the SOM configuration is evaluated primarily in E3SMv2 model, SOM experiments are also performed in which the SOM forcing fields are derived from the previous E3SMv1 (Golaz et al., 2019) and CESM1 fully coupled simulations (Hurrell et al., 2013).

The SOM formulation and the method of deriving prescribed ocean heat convergence (OHC) and mixed layer depth (MLD), and the motivation for our choices of these fields (the SOM configuration) for the study are discussed next. The E3SMv2-SOM formulation is the same as the "NEWSOM" formulation described in (Bitz et al., 2012) which

is currently used in the CESM model, which replaces an alternate treatment used in early versions of CESM referred to as "OLDSOM" formulation in the study. Here, the equations for computing the prescribed OHC and temperature evolution in the SOM are implemented on the MPAS grid and E3SM architecture. Note that the term "mixed layer depth" is used interchangeably with the term "boundary layer thickness" in this study. The ocean mixed layer depth and boundary layer thickness both represent the well mixed, homogeneous ocean surface layer, but are computed differently in the ocean model. However, to avoid confusion, the more widely used ocean mixed layer depth is what is used throughout the rest of the paper.

The NEWSOM formulation was designed to reproduce SSTs and sea ice from a fully coupled model climatology, unlike the "OLDSOM" and other SOM formulations have been used with a target of reproducing observed SSTs and sea ice climatology (Knutson, 2003; Schmidt et al., 2006; McFarlane et al., 1992). These earlier methods for deriving the prescribed OHC involve restoring surface heat fluxes or SSTs in the SOM to the observed climatology. However, online adjustments to the OHC were often necessary in order to reproduce observed SSTs and sea ice climatology and avoid excessive sea ice growth and cooling. The advantage of the NEWSOM formulation over the earlier treatments is that it does not require online adjustments to the prescribed OHC in order to reproduce the intended SSTs and sea ice thickness climatology. Nevertheless, this SOM formulation can inherit biases from the fully coupled model from which it is derived. All SOM models also can suffer from potential biases due to the lack of mechanical coupling with the atmosphere and the seasonally invariant ocean MLD.

The SOM formulation simulates the ocean mixed layer/surface temperature following equation (1).

$$\begin{aligned} \rho_o C_p h \frac{\partial T}{\partial t} &= F_{oa} + F_{oi} - F_o \\ F_{oi} &= l_h (T_{frz} - T) \end{aligned} \tag{1}$$

Here h is the spatially varying annual climatological ocean MLD and T is the ocean mixed layer temperature. F_{oa} is the air-sea heat flux exchange between the atmosphere and ocean; F_{oa} includes the radiative short wave and long wave, and the turbulent sensible and latent heat flux components. F_{oi} is the ocean-to-ice heat fluxes for sea ice melt and frazil ice growth, while F_o is the ocean heat convergence (OHC). The constants ρ_o, C_p and l_h are the density, heat capacity of sea water and latent of freezing, respectively.

The variables T, F_{oa}, and F_{oi} in equation (1) are computed online in the SOM configuration. T and frazil component of F_{oi} are primarily computed in the SOM, while the air-sea fluxes are computed from the coupling of the atmosphere model with the SOM temperature. The frazil component of the ocean-to-ice heat fluxes is the heat released when frazil ice forms. It is computed according to equation (1b), anywhere the ocean temperature falls below the freezing temperature in the SOM, after which the ocean temperature is reset to the freezing temperature. The melt component of the ocean-to-ice heat fluxes are computed similarly but in the sea ice model, anywhere there is sea ice and the ocean temperature is above freezing. The ocean temperature, frazil and melt ocean-to-ice heat fluxes are thus exchanged between the sea ice model and the SOM.

Monthly climatological OHC (F_o), on the other hand, is prescribed for the SOM since it does not simulate ocean circulation and the heat transport associated with it. Note that although ocean heat convergence and heat transport are sometimes used interchangeably, they are different quantities, OHC is a scalar quantity representing the convergence of the ocean heat transports (lateral fluxes) across each face of the ocean grid cell. F_o is computed from a quasi-equilibrium climatological state of a fully coupled ocean model, as a residual of the monthly climatological air-sea fluxes, ocean-to-ice heat

fluxes, and ocean mixed layer heat content tendencies, following equation (2). As in the SOM equation 1, a time-invariant annual climatological MLD (h) is also used in computing the F_o in equation 2. Using a quasi-equilibrium or equilibrium state of the fully coupled model ensures that the global and time average of the F_o is as close as possible to zero. In equilibrium the ocean is in steady state, and heat exchange between the ocean MLD and deep ocean goes to zero in the global and time average. Further adjustment is also applied to the computed F_o to ensure the global and time average ocean heat convergence is zero, so that F_o cannot act as source or sink of heat in the SOM simulation. F_o at each time step in the SOM simulation is interpolated from the prescribed monthly climatological OHCs and this process is repeated annually.

$$F_o = -\rho_o C_p h \frac{\partial T}{\partial t} + F_{oa} + F_{oi} \tag{2}$$

2.1 Experiments

A suite of 50-yr long SOM experiments are run to evaluate the ability of the E3SMv2-SOM to reproduce the fully coupled E3SMv2 climatology and equilibrium climate sensitivity, as well as to test the impact of the prescribed ocean heat convergence on the baseline climate simulated by the SOM. In order to evaluate the ability of the SOM to reproduce the climatology of the fully coupled pre-industrial control experiment at low resolution (v2.LR.control), an analogous SOM experiment (SOM.v2.LR-OHC) is run. The SOM.v2.LR-OHC experiment is similar to the fully coupled v2.LR.control experiment except that the MPAS-O model is replaced with the SOM, other model components (that is EAMv2, ELM, MPAS-SI and MOSART) are identical. Both simulations are forced with 1850 pre-industrial atmosphere and land conditions and the prescribed OHC and MLD for the SOM.v2.LR-OHC experiment are also derived from the quasi-equilibrium climatology period (Years 481-500) of the v2.LR.control experiment. The SOM simulation is also initialized from the January climatological SSTs from this time period (Figure 1).

In order to test the sensitivity of E3SMv2 model to the strength of the heat transports in the ocean, three additional SOM experiments (SOM.v1.LR-OHC, SOM.v1.HR-OHC and SOM.P-OHC) are run using different choices for the prescribed OHC. The OHCs prescribed for the SOM.v1.LR-OHC, SOM.v1.HR-OHC and SOM.P-OHC experiments are derived from the fully coupled E3SMv1 control simulations at Low (v1.LR.control) and high resolutions (v1.HR.control), and CESM control simulation, respectively (See Table 1 for a summary of the experiments).

These three fully coupled simulations are chosen primarily because of the strengths of the Atlantic Meridional Overturning Circulation (AMOC) in their ocean models. The AMOC is a major means of poleward heat transport by the ocean, which has great impact on the global climate. When compared to observations, the v1.LR.control and v2.LR.control simulations have very similar but weak AMOC (12 and 11 Sv, respectively; Golaz et al., 2019, 2022), while v1.HR.control and CESM control experiments have similar strong AMOC (18 and 20 Sv, respectively; Caldwell et al., 2019). The impact of the AMOC strength in these fully coupled simulations can be seen on the respective OHCs that are derived from them (Figures 2). When compared to those of the v2.LR.control and v1.LR.control, the OHCs derived from the v1.HR.control and CESM fully coupled experiments show much greater heat convergence over the subpolar Atlantic, and over the polar regions of Southern Ocean, due to their stronger AMOC (compare Figures 2b, c, and 1a, 2a). The relationship between the prescribed OHCs and the poleward ocean and atmospheric heat transports is discussed further in the section 3.2. By using a pair of SOM experiments with similar ocean heat transports from different generation of models (E3SMv1-LR/E3SMv2-LR and E3SMv1-HR/CESM), we are able to verify the robustness of the impact of ocean heat transport strength on the climate response.

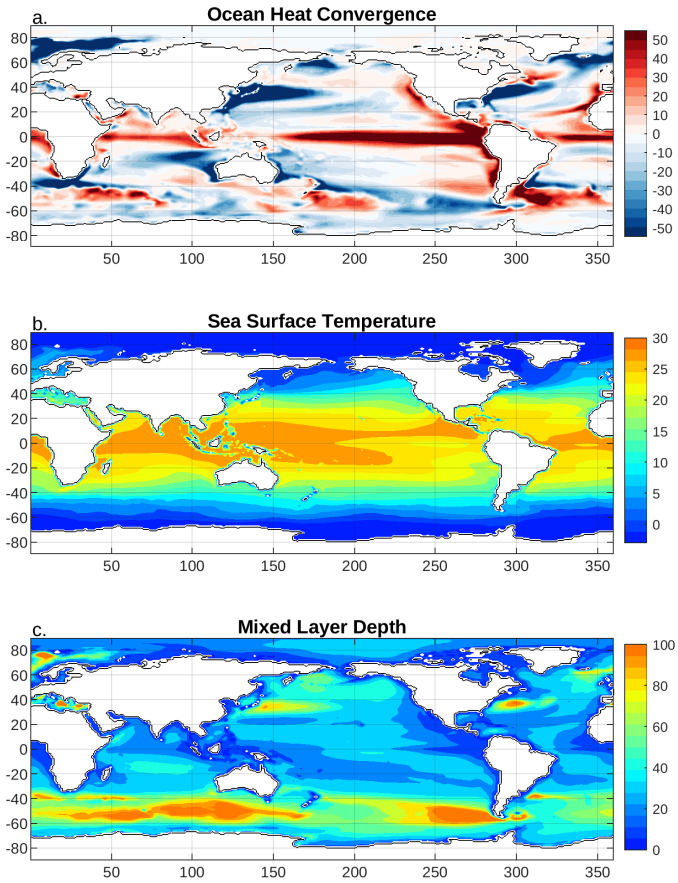

Figure 1. Annual climatological forcings diagnosed from years 481 - 500 of the MPAS Ocean model output of the fully coupled v2.LR.control simulation, and prescribed for the SOM.v2.LR-OHC simulation; (a) Ocean Heat Convergence (Wm^{-2}; Positive sign = heat divergence and negative sign = heat convergence), (b) Sea Surface Temperature (°C) and (c) Mixed Layer Depth (m),

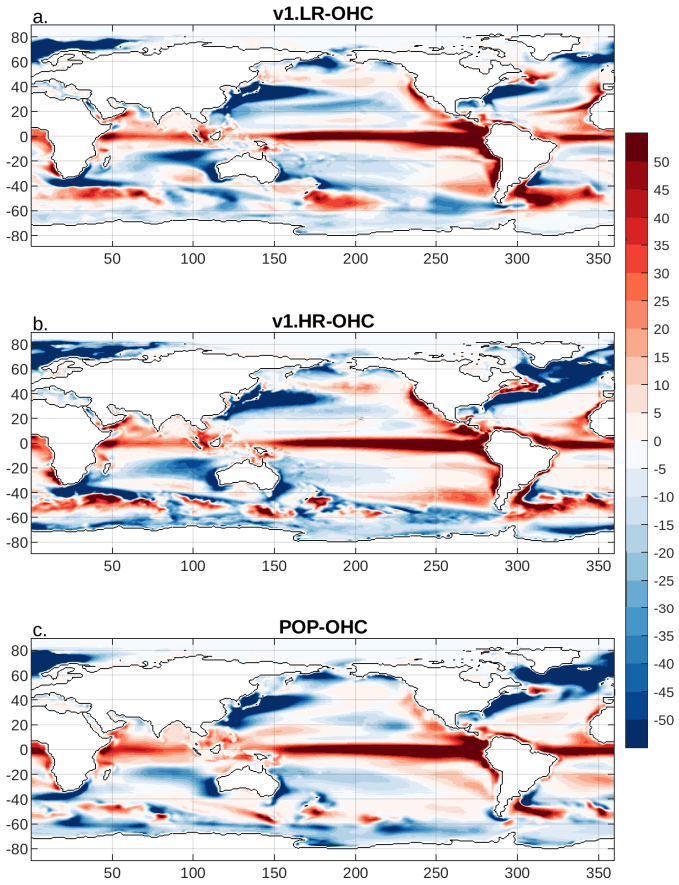

Figure 2. Ocean heat convergence (W/m^2) diagnosed from the fully coupled E3SMv1 control simulations with MPAS-ocean model at (a) Low resolution (v1.LR.Control), (b) High resolution (v1.HR.Control), and (c) CESM simulation with POP ocean model. Negative sign is ocean heat convergence into the ocean mixed layer

Table 1. Summary of Experiments

Name	Forcings	Length
SOM.v2.LR-OHC	1850 forcing and initialization; Prescribed ocean heat convergence derived from the fully coupled E3SM v2.LR.control experiment.	50 yrs
SOM.v1.LR-OHC	1850 forcing and initialization; Prescribed ocean heat convergence derived from the E3SM v1.LR.control experiment.	50 yrs
SOM.v1.HR-OHC	1850 forcing and initialization; Prescribed ocean heat convergence derived from the fully coupled E3SM v1.HR.control experiment.	50yrs
SOM.P-OHC	1850 forcing and initialization; Prescribed ocean heat convergence derived from the fully coupled CESM control experiment.	50yrs
SOM.v2.LR-OHC-4xCO_2	4xCO_2 forcing; initialized from year 25 of the SOM.v2.LR-OHC experiment; Prescribed ocean heat convergence derived from the fully coupled E3SM v2.LR.control experiment.	50yrs
SOM.v1.HR-OHC-4xCO_2	4xCO_2 forcing; initialized from year 25 of the SOM.v1.HR-OHC experiment; Prescribed ocean heat convergence derived from the fully coupled E3SM v1.HR.Control experiment.	50yrs

Aside from the differences in their AMOC strengths, there are other significant differences among the fully coupled simulations chosen for deriving the prescribed OHCs. The model configurations used to produce v1.LR.control and v2.LR.control fully coupled experiments contain significant differences in their atmospheric model component, though they used similar 1850 preindustrial forcing conditions, while the v1.HR.control simulation had the same model components as the v1.LR.control experiment, but used a much finer grid resolution for all model components, as well as 1950 forcings and different choices for atmospheric model tuning from the v1.LR.control simulations (Caldwell et al., 2019). The fully coupled CESM experiment also contains different model components from the E3SM experiments and uses 1850 settings for atmosphere and land forcings. Despite the various differences, our goal in running this set of SOM experiments is to study the sensitivity of the E3SMv2 baseline climate, only to the differences in ocean heat transports in these fully coupled experiments. We achieved this by using a single choice of atmosphere, ice, and land models (i.e E3SMv2 configuration), with a single SOM formulation (using different choices for prescribed OHC) for all four SOM experiments. The SOM experiments also use the same 1850 atmospheric forcings and ocean MLD, and are initialized from the same initial ocean state, such that the only difference between these SOM experiments is their prescribed OHC.

Another set of CO_2 quadrupling SOM experiments (SOM.v2.LR-OHC-4xCO_2, and SOM.v1.HR-OHC-4xCO_2) is run in order to evaluate the equilibrium climate sensitivity of the E3SMv2 model to CO_2 forcing and test its sensitivity to prescribed ocean heat transport. The SOM.v2.LR-OHC-4xCO_2 and SOM.v1.HR-OHC-4xCO_2 are initialized from years 25 of the SOM.v2.LR-OHC and SOM.v1.HR-OHC control simulations respectively with quadrupled CO_2 level (See Table1).

3 Results

3.1 Comparison between fully coupled and SOM experiments

The ability of the E3SMv2-SOM to reproduce the fully coupled model climate is first evaluated by comparing the equilibirum climate of the E3SMv2-SOM (years 26-50 of SOM.v2.LR-OHC experiment) with that of its fully coupled analogue (years 481-500 of the v2.LR.control experiment; Note that the SOM simulation reaches an equilibrium within 20 years). Recall that the target climatology for the SOM.v2.LR-OHC experi-

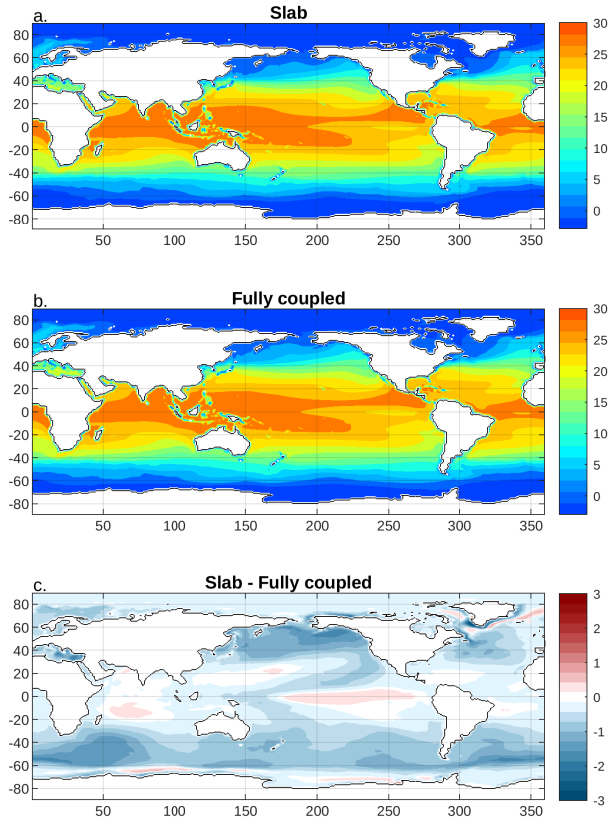

Figure 3. Annual mean Sea Surface temperature ($^{\circ}C$) in the SOM.v2.LR-OHC slab ocean experiment (a), and v2.LR.piControl Fully coupled preindustrial control experiment (b) and their difference (c). Pattern correlation between the SOM and fully coupled SST patterns is 1.

ment is the v2.LR.control fully coupled experiment's climatology, since its prescribed OHC, MLD and initial temperature are derived from the v2.LR.control experiment.

3.1.1 Climatology

The annual averaged sea surface temperature in the SOM.v2.LR-OHC experiment shows very good agreement with that of its corresponding fully coupled experiment (Figure 3 a and b), with a pattern correlation of 1. SSTs in the SOM.v2.LR-OHC experiment are overall cooler than those of the fully coupled experiment, particularly in subpolar regions in both hemispheres, while it is warmer in tropics, particularly in the Pacific(Figure 3c). This cold bias is greater in the summer season in each hemisphere, that is, DJF months in the Southern hemisphere and JJA months in the Northern hemisphere (Figures S1 and S3). As a result, the global annual surface air temperature simulated in the SOM experiment is less than 0.5° colder than that of the fully coupled experiment. The global averaged surface air temperature for the equilibrium state of the SOM experiment is 13.2°C, compared to 13.7°C in the fully coupled control experiment (Golaz et al., 2022).

The SST anomaly pattern might be explained by the annual ocean MLD that is used in deriving the prescribed OHC and subsequently used for the SOM experiment. Recall that the prescribed OHC is computed with the annual climatological MLD rather than a seasonally varying monthly climatological one. The ocean mixed layer is deep-

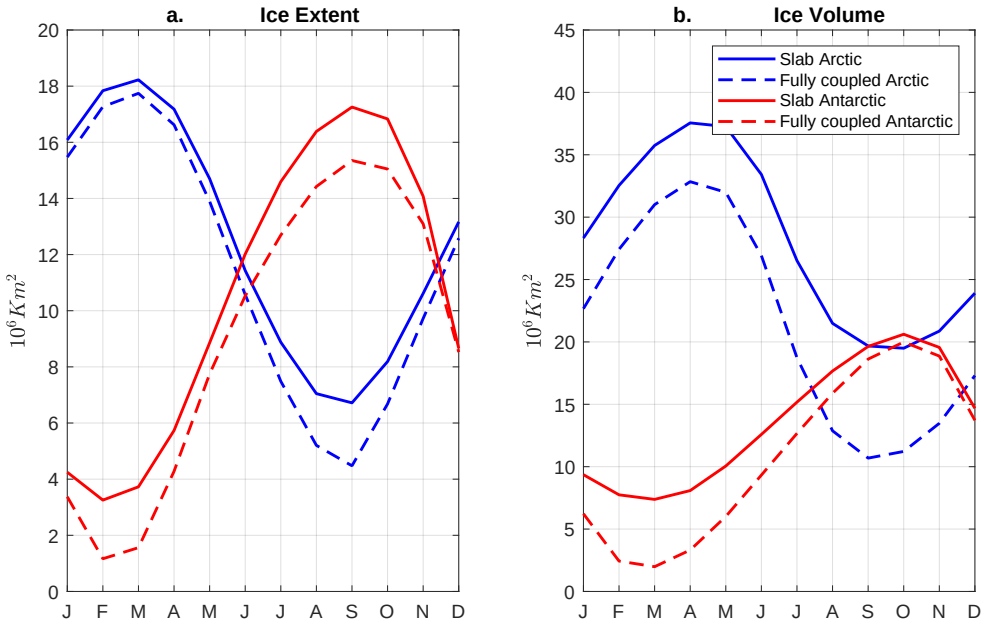

Figure 4. Climatological Sea ice extent (a) and sea ice volume in the SOM.v2.LR-OHC experiment (Years 26 -50; solid line) and v2.LR.Control fully coupled experiment (Years 481 - 500; dashed lines), in the Arctic (Blue) and Antarctic (Red).

est and exhibits more seasonal variation in the subpolar regions in both hemispheres. The MLD deepens in winter and shallows in summer of each hemisphere. The annual mean MLD at a given location is therefore deeper than the monthly MLD in the summer season and shallower in winter. As a result, using an annual mean MLD in the SOM causes an underestimation of the temperature tendency in summer and in an overestimation in winter, according to equation (1). This might explain why the cold bias is greater in summer than in winter of each hemisphere.

As a result of the cold bias in surface temperature, the SOM generally simulates greater sea ice extent and thickness than the fully coupled experiment. However, the bias in the sea ice extent is smaller than that of sea thickness, especially in the Arctic (Figure 4). Sea ice thickness bias is the largest in the shoulder seasons (SON in the Arctic and MAM for the Antarctic), when the climatological Sea ice thickness and extent are at their minimum. Greater sea ice thickness bias in the shoulder seasons is consistent with the greater SST cold bias that is simulated in the preceding summer seasons in the SOM. (Figure 4). The results here show a good agreement with the CESM-SOM comparison described in Bitz et al. (2012).

Precipitation is also reproduced reasonably well in the SOM experiment, with a global mean bias that is less than 1 percent of the fully coupled global precipitation average (Figure 5). However, precipitation in the SOM experiment is generally less than the fully coupled experiment, with the exception of a stronger precipitation bias in the tropics, particularly over the western tropical Pacific. This precipitation bias pattern can be explained by the SSTs anomaly pattern in the SOM experiment, compared to the v2.LR.piControl experiment. It also appears that the the double ITCZ bias in the SOM is reduced compare to the v2.LR experiment.

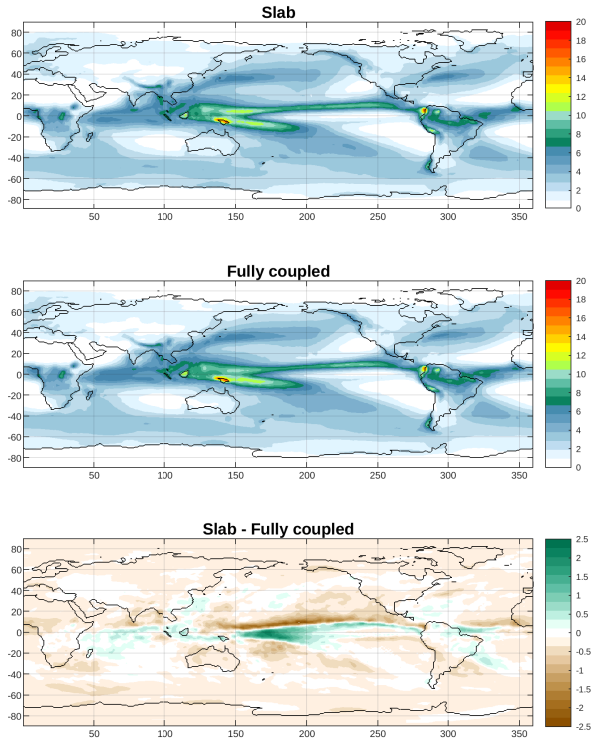

Figure 5. Annual mean Precipitation (mm/day) in the SOM.v2.LR-OHC slab (top) and v2.LR.piControl fully coupled (middle) experiments, and their difference (bottom).

3.2 Sensitivity to ocean heat transports

The capability of evaluating the impact of various prescribed OHCs on climate is another valuable use of the SOM. Here, the sensitivity of the E3SMv2 baseline climate to various ocean heat transport strengths is evaluated by comparing the SOM.v2.LR-OHC with the SOM.v1.LR-OHC, SOM.v1.HR-OHC and SOM.P-OHC experiments. Recall that the prescribed OHCs are the only differences among these four SOM experiments (section 2.1), and these are chosen based on the AMOC strengths of the fully coupled simulations from which the OHCs are derived. The global and annual averages for these prescribed OHCs are also zero, by design (See section 2), so that the climate responses to the OHCs occur only as a result of the differences in their spatial pattern and local amplitude.

The differences between the OHCs prescribed for the SOM.v2.LR-OHC experiment and each of the other three SOM experiments are shown in Figure 6. OHC anomalies in the other three SOM experiments are defined with respect to the SOM.v2.LR-OHC experiment. Similar to their AMOC strengths, the OHC differences between the SOM.v2.LR-OHC and SOM.v1.LR-OHC experiment are small, while those of the SOM.v1.HR-OHC and SOM.P-OHC experiments are much greater, particularly over the subpolar Atlantic and in Southern Ocean. Recall that the AMOC strengths of the v1.LR.control and v2.LR.control is similar and weak, while AMOC of v1.HR.control and CESM-POP are both stronger. Because the global averages of the OHCs are zero, the increased ocean heat convergence in Northern and Southern subpolar/Polar regions in the SOM.v1.HR-OHC and SOM.P-OHC experiments are also compensated by increased heat divergence in the subtropical/tropical regions.

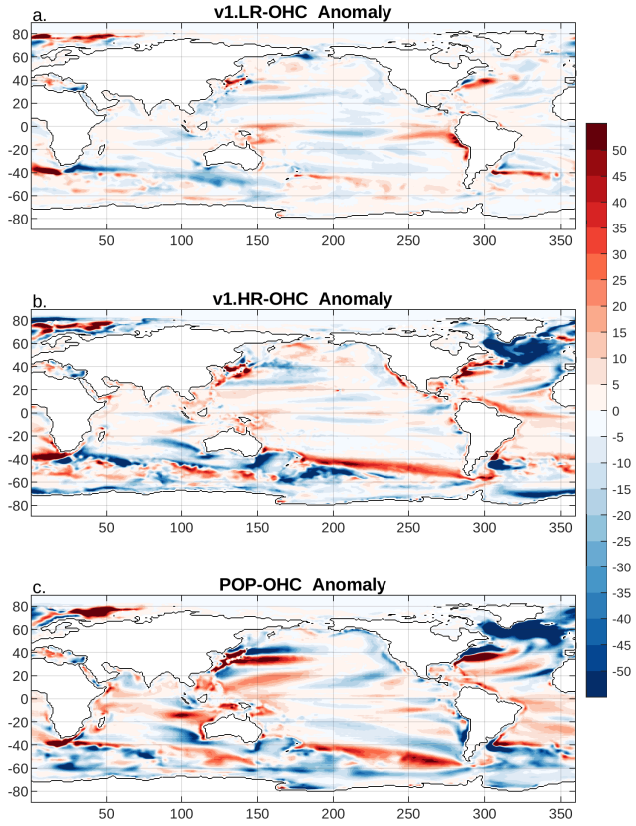

Figure 6. Differences between the ocean heat convergences derived from the E3SM fully coupled v2.LR.control simulation and the (a) v1.LR.control (v1.LR-OHC), (b) v1.HR.control (v1.HR-OHC) and (c) CESM control (POP-OHC) simulations. Anomalies represent differences between the experiments. Negative sign indicates more heat convergence and positive is less heat divergence

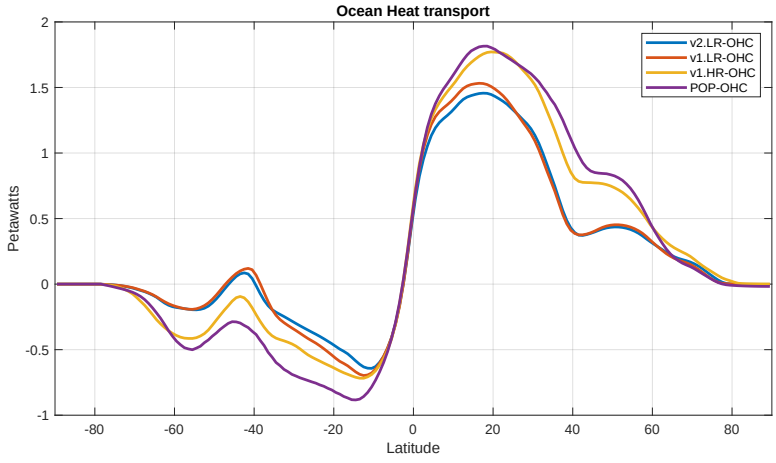

Figure 7. Poleward Ocean heat transports computed from the prescribed ocean heat convergence forcings for the SOM.v2.LR-OHC (blue) SOM.v1.LR-OHC, (orange), SOM.v1.HR-OHC (Yellow) and SOM.P-OHC (purple) experiments. Positive sign denotes northward heat transport and negative sign denotes Southward heat transport.

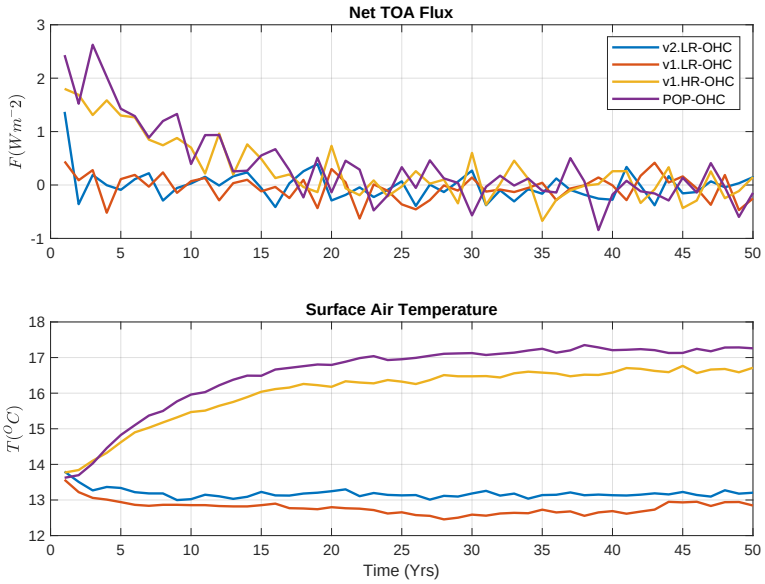

Figure 8. Annual and Globally averaged Top of the Atmosphere heat flux (Wm^{-2}; Top) and surface air temperature ($^{\circ}C$; bottom) in the SOM.v2.LR-OHC (blue), SOM.v1.LR-OHC (orange), SOM.v1.HR-OHC (yellow), SOM.P-OHC (purple) experiments.

Apart from their AMOC strengths, another metric that can quantify the strengths of the ocean heat transport in the fully coupled experiments that produce these OHC patterns is their poleward ocean heat transport. The poleward OHT can be computed from the prescribed OHCs as $\int\int F_o(y)dxdy$ (Figure 7). Similar to the differences in their AMOC strengths, the prescribed OHCs for both SOM.v1.HR-OHC and SOM.P-OHC exhibit greater poleward heat transport in both Northern and Southern hemispheres than those in SOM.v1.LR-OHC and SOM.v2.LR-OHC. The SOM.v1.LR-OHC and SOM.v2.LR-OHC experiments are thus hereafter referred to as the low-OHT forcing experiments, while the SOM.v1.HR-OHC and SOM.P-OHC as the high-OHT forcing experiments.

Consistent with their fast equilibration time, there is an initial increase in the net global TOA flux, which quickly reduces to zero after about 20 years in all the SOM experiments (Figure 8). The low-OHT forcing experiments have similar weak initial TOA forcing response and surface air temperature responses, while the high-OHT forcing experiments also have a similar large initial TOA forcing of about 2 Wm^{-2}. The equilibrium global surface air temperatures in the low-OHT experiments are also similar, with a difference of about 0.5°C between the SOM.v2.LR-OHC and SOM.v1.LR.OHC experiments (13.2°C and 12.7°C); those of the high-OHT experiments are also close in value (17^oC and 16.6^oC). However, the surface temperature response difference between the two pairs of low and high-OHT experiments is significant. The difference between the equilibrium time (Years 25 - 50) and globally averaged surface air temperature in the low-OHT and high-OHT experiments, is about 4°C. This low/high-OHT temperature difference is almost the same as the equilibrium global surface temperature response to CO_2 doubling as estimated with the fully coupled E3SMv2 (Golaz et al., 2022).

It is noteworthy also, that the high-OHT SOM simulations are also warmer than the fully coupled simulation from which their OHCs are derived from, despite sharing the same ocean heat transports. For example, the surface temperature in the v1.HR.control fully coupled experiment is about 14.1°C, which is much cooler than the 16.6°C in the

SOM.v1.HR-OHC experiment. However, this transition to another climate in the high-OHT SOM simulations (relative to the fully coupled simulations their OHCs are derived from) can be anticipated, since the fully coupled simulations are produced by different atmosphere/land model components, with different parameter tunings, and exogenous forcing (by greenhouse gases, land use and land cover change, etc.). The atmosphere model in the v1.HR.control simulation (EAMv1) is different from the EAMv2 used in the SOM.v1.HR-OHC experiment here, with significant differences in their parameter tunings (Golaz et al., 2022). Our testing of the SOM configuration in E3SMv1 (not shown) indicates that the SOM experiments with the EAMv1 atmosphere were generally cooler than those of EAMv2. Different parameter tunings are also used for the low and high resolution fully coupled v1.HR.control and v1.LR.control simulations with EAMv1. In the Caldwell et al. (2019) study, the LR fully coupled simulation was compared with another LR fully coupled simulation that uses the HR atmosphere model parameter tunings applied (LR-tunedHR); it was found that surface temperature in the LRtunedHR simulation is cooler than the LR simulation. This result indicates that the HR parameter tuning of v1.HR.control fully coupled experiment helps to reduce the surface temperature in this experiment. The v1.HR.control experiment further uses year-1950 atmospheric and land forcings which produces relatively more negative TOA forcing compared to the year-1850 forcings used for the SOM.v1.HR-OHC here.

Similarly, the CESM fully coupled simulation also uses very different atmosphere and land model components (CAM5, CLM45) with different parameter tuning than the EAMv2 and ELM model components used in the SOM.P-OHC simulation here. Our SOM test with E3SMv1 also allows the option of using either CAM5 or EAMv1 atmospheric component, and the SOM experiment with CAM5 and CLM45 also produces much cooler surface temperatures (not shown). As a result of these different factors, it is reasonable to expect that the climate in the SOM.v1.HR-OHC and SOM.v1.P-OHC simulations are warmer than their derivative fully coupled experiments, and a fruitful comparison between these SOM experiment and the fully coupled one cannot be made. Only the comparison of the SOM.v2.LR-OHC experiment to its fully coupled counterpart makes sense because of the similar model components and forcings they share. Nevertheless, comparing these four simulations is useful for understanding the impact of ocean heat transport strength on a baseline climate.

The large global surface temperature difference between the low-OHT and high-OHT experiments occurs largely over the subpolar regions in both hemispheres, while the subtropics and tropics show much weaker surface temperature response (Figure 9e, f). These SST patterns are largely explained by their OHC forcing difference patterns; similar to the SST response patterns, ocean heat convergence strengthens mainly in the subpolar North Atlantic and Southern Ocean in the high-OHT experiments, while ocean heat divergence strengthens in the subtropical and tropical regions (compare Figures 6 b, c and 9 e, f). However, there are also significant differences between the anomalous SST and OHC patterns in the high-OHT experiments. The warming response over the northern subpolar Pacific is comparably large even though the OHC strengthening there is weak and even decreases in some locations. SST response in the Southern hemisphere is also generally greater the Northern one, even though the OHC strengthening there is weaker. The maximum surface air temperature response occurs poleward of 50°S over the Antarctic (Figure10), in spite of the prescribed OHC forcing being generally weaker in the Southern hemisphere (compare Figures 7 and 10). The global cooling response in the SOM.v1.LR-OHC experiment also occurs largely over the subpolar Southern ocean despite having very similar ocean heat transport with the SOM.v2.LR-OHC experiment (Figure 9d and 10). These differences between the surface temperature response and OHC forcing patterns suggests the atmosphere also plays a role in the surface temperature response.

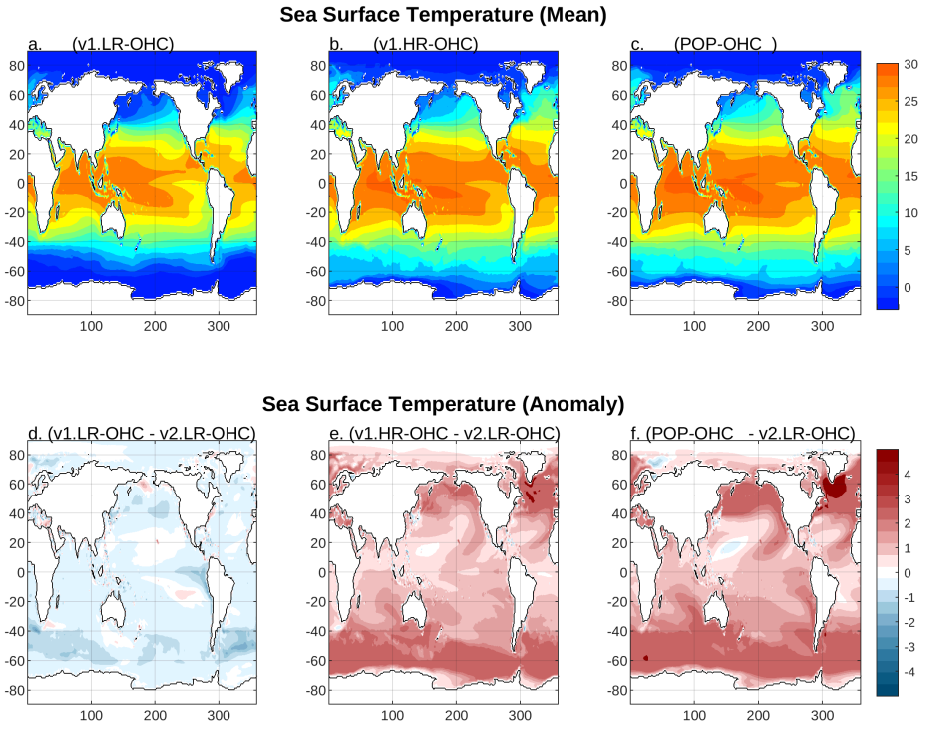

Figure 9. Climatological mean SSTs for years 26 - 50 in the SOM.v1.LR-OHC (a), SOM.v1.HR-OHC (b) and SOM.POP-OHC (c) experiments and their anomalies from the climatological mean SST in the SOM.v2.LR-OHC (e -f).

As a result of their surface temperature response and patterns, sea ice extent and volume are different between the experiments (Figure 11). While Sea ice extent/volume are generally much smaller in the high-OHT than low-OHT experiments, sea ice extent/volume is greatest in SOM.v1.LR-OHC experiment due to its cooler surface temperature. Sea ice becomes seasonal in the high-OHT experiments, disappearing particularly in the shoulder seasons. The percentage increase/decrease in Antarctic sea ice extent/volume is greater than those of the Arctic in the low/high-OHT experiments, due to the greater surface temperature response in the Southern Ocean.

It is noteworthy, that Arctic sea ice extent shows the least variation among all four experiments, particularly between experiments with similar prescribed OHCs, while Arctic sea ice volume and Antarctic extent/volume vary a lot more among the experiments (compare Figure 11a, with b, c, d). As a result of their very similar OHCs, Arctic sea ice extent, is almost the same between the two low-OHT experiments, as well as high-OHT experiments. Similarly, when compared to the fully coupled simulation its OHC is derived from, Arctic sea ice extent maximum in the SOM.v1.HR-OHC experiment is much closer to that of the fully coupled v1.HR.control experiment, its prescribed OHC is derived from (12.5 vs $16\text{x}10^6 Km^2$; (Caldwell et al., 2019), despite the large surface temperature difference between them. The Antarctic sea ice extent and volume in the SOM.v1.HR-OHC simulation, on the other hand, are much smaller than those of the v1.HR.control experiment (5 vs $17.5\text{x}10^6 Km^2$). These results support the earlier shown idea that Arctic sea ice extent is largely controlled by frazil ice growth, which in turn is controlled by the ocean heat convergence. As a result, experiments with similar OHCs can produce similar Arctic sea ice extent even with differences in the Atmosphere model. Arctic sea ice thickness, on the other hand, is largely controlled by the atmosphere through basal

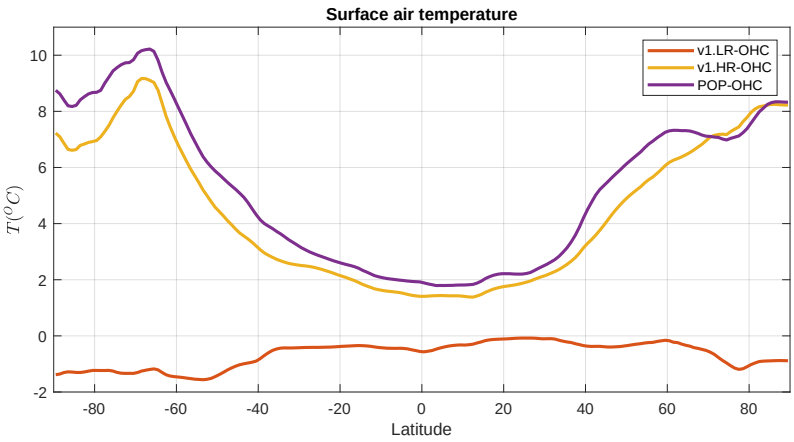

Figure 10. Zonally averaged anomalous surface air temperature in the SOM.v1.LR-OHC, SOM.v1.HR-OHC and SOM.P-OHC experiments. Anomalies are defined with respect to the climatology of the years 25 -50 in the SOM.v2.LR-OHC experiment

ice growth, and thus responds more surface air temperature changes. Similarly, Antarctic sea ice extent/volume is largely controlled by the atmosphere through ice growth from snowfall (Garuba et al., 2020).

The changes in surface temperature described above, also cause changes in the meridional temperature gradient in the atmosphere, which then cause poleward atmospheric heat transport (AHT) to respond to and compensate for the systematic prescribed changes in OHC/OHT in all three experiments (Figure 12a comparing dashed and solid lines). The increase in prescribed poleward OHT in the high-OHT experiments is compensated by a decrease in poleward AHT everywhere except for the polar regions. At the polar regions, there is an increase in poleward AHT in the two high-OHT experiments, despite having negligible OHT anomalies there. This compensation between poleward OHT/AHT also occurs in the SOM.v1.LR-OHC experiment, that is, decrease in poleward OHT is compensated by increase in poleward AHT, though the anomalies are much weaker in this experiment. It is noteworthy that the rate of compensation between poleward AHT and OHT is also different in each hemisphere. The prescribed anomalous poleward OHT is almost perfectly compensated by anomalous poleward AHT in the Northern hemisphere, while in the Southern hemisphere, OHT changes are overcompensated by the AHT in all three experiments. This overcompensation is the largest around 40^{o}S in the SOM.v1.HR-OHC experiment, where reductions in the poleward AHT overcompensates the OHT increases by a factor of 2. This overcompensation in the Southern hemisphere is likely associated with the greater surface temperature response and sensitivity to the prescribed OHC there, which causes greater decrease in the meridional temperature gradient there.

The poleward AHT response can be decomposed further into components that are contributed by the zonally integrated surface and Top of the Atmosphere (TOA) heat fluxes. The net of these two quantities is the zonally integrated Atmospheric Heat Convergence (AHC; $\int F_a dx$), which is integrated meridionally to give the atmospheric heat transport. We compare the AHC response and its components to the prescribed zonally integrated OHC anomalies ($\int F_o dx$) in the experiments (Figure 12b, c and d; Note that the heat convergence variables are multiplied by dy to convert the zonally integrated units from Wm^{-1} to W for consistency with heat transport units in panel a). Anomalies here are also defined with respect to the SOM.v2.LR-OHC experiment.

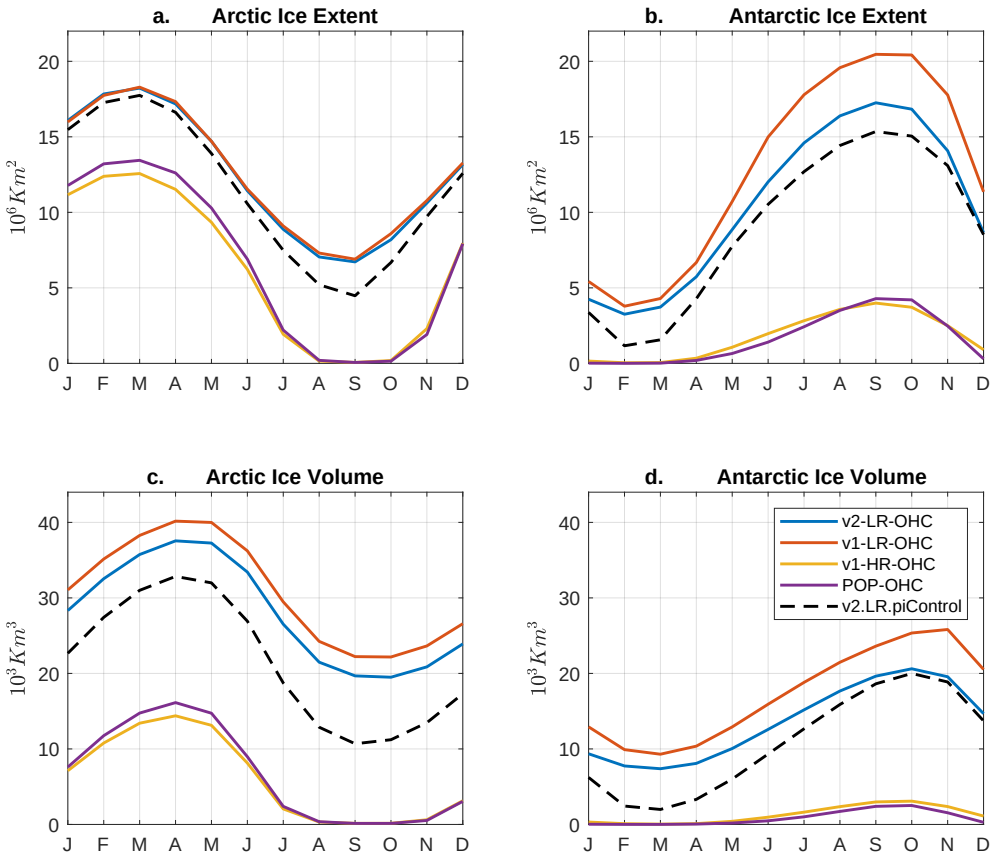

Figure 11. Sea ice extent and volume in the Arctic (a, c) and Antarctic (b, d) in the SOM.v2.LR-OHC (blue), SOM.v1.LR-OHC (orange), SOM.v1.HR-OHC (yellow) and SOM.P-OHC (purple) and fully coupled v2.LR.piControl (dashed line) experiments

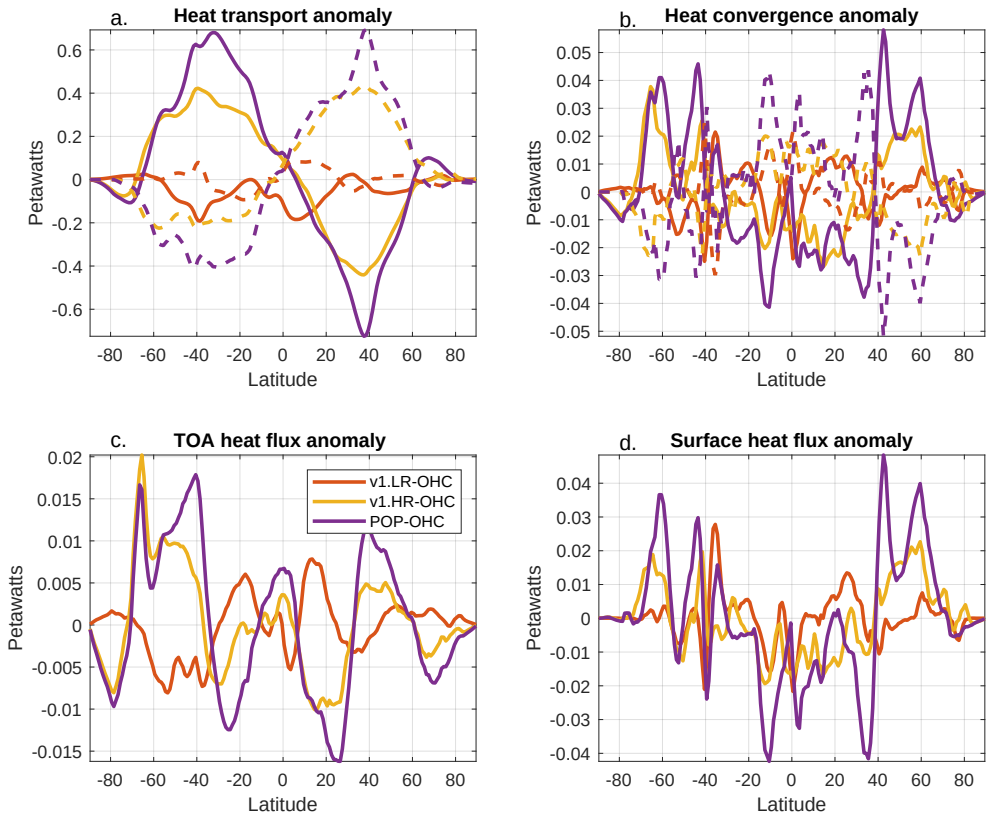

Figure 12. (a) Anomalous heat transport in the atmosphere (solid) and ocean (dashed). (b) Zonally integrated anomalous heat convergence in the atmosphere (solid) and ocean (dashed), and (c) the contributing anomalous net TOA and (d) net surface heat fluxes in SOM.v1.LR-OHC (orange), SOM.v2.LR-OHC (yellow) and SOM.P-OHC(purple) experiments; Anomalies are defined with respect to corresponding values in the SOM.v2.LR-OHC experiment. Note that the zonally integrated heat flux and convergence quantities (Wm^{-1}) are again multiplied by dy to convert units to Petawatts)

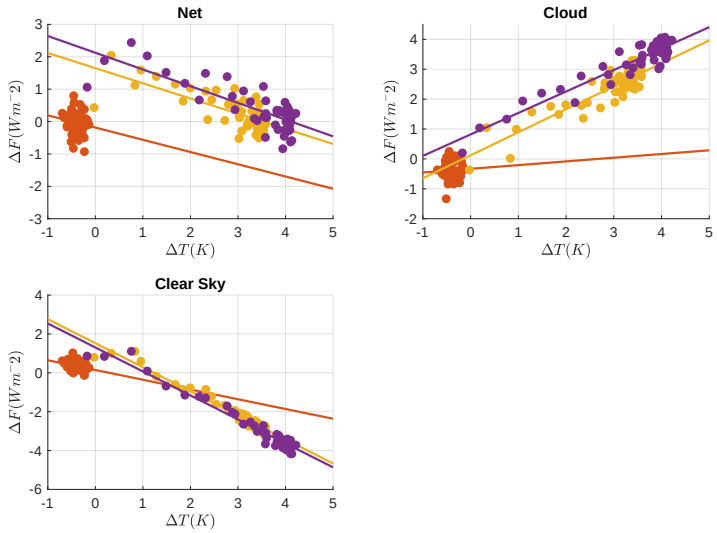

Figure 13. Regression of the annual global anomalous surface air temperature against anomalous net top-of-the-atmosphere radiative fluxes (a), and its net cloud (b) and clear-sky components (c) in the SOM.v1.LR-OHC (orange), SOM.v1.HR-OHC (yellow) and SOM.P-OHC (purple) experiments. Anomalies are taken with respect to the values in the SOM.v2.LR-OHC experiments.

The AHC and OHC show similar meridional variation pattern, however, their magnitudes are different (Figure 12b solid and dashed lines; negative sign in OHC means net gain of heat by the mixed layer). Like the poleward AHT response, the magnitudes of the AHC and OHC forcing are largely the same in the northern hemisphere, but greater in the Southern hemisphere subpolar regions. The AHC response is greater than the OHC forcing between 40-70°S in all the experiments. Comparing the contributions of the surface and TOA heat flux components of the AHC response suggests, that this overcompensation in the AHC/AHT is largely associated with a large TOA flux response in the regions of overcompensation (Figure 12c, d solid lines). While AHC's meridional pattern and magnitude is largely contributed by the surface heat flux component, the differences between the AHC and OHC magnitude is contributed TOA heat flux pattern and magnitude. The surface heat flux pattern and magnitude almost exactly matches that of the prescribed OHC forcing, such that the residual of the AHC and OHC is mainly contributed by the TOA flux component. Unlike the surface heat flux pattern and OHC forcing's meridional pattern, the anomalous TOA is greater in the subpolar southern hemisphere than the northern one. Similarly over the polar regions, there is a relatively large TOA response even though there is a negligible anomalous surface heat flux increase. This result suggests that the overcompensation of the between the OHT and AHT in the Southern hemipshere and the large surface temperature sensitivity to prescribed OHC there, as well over the polar regions is likely caused by atmospheric feedbacks (e.g., clouds, water vapor and lapse rate) rather than by the local increase in surface heat fluxes.

A regression of the global anomalous TOA fluxes and their components against the global anomalous surface air temperature in the three slab experiments (Figure 13), further suggests that the large positive anomalous TOA in the high-OHT experiments can be attributed to the cloudy component response. Initially, responses in both clear-sky and cloudy components produce a positive TOA forcing in the first four years. However, the TOA forcing due to the clear-sky component quickly becomes negative after four years,

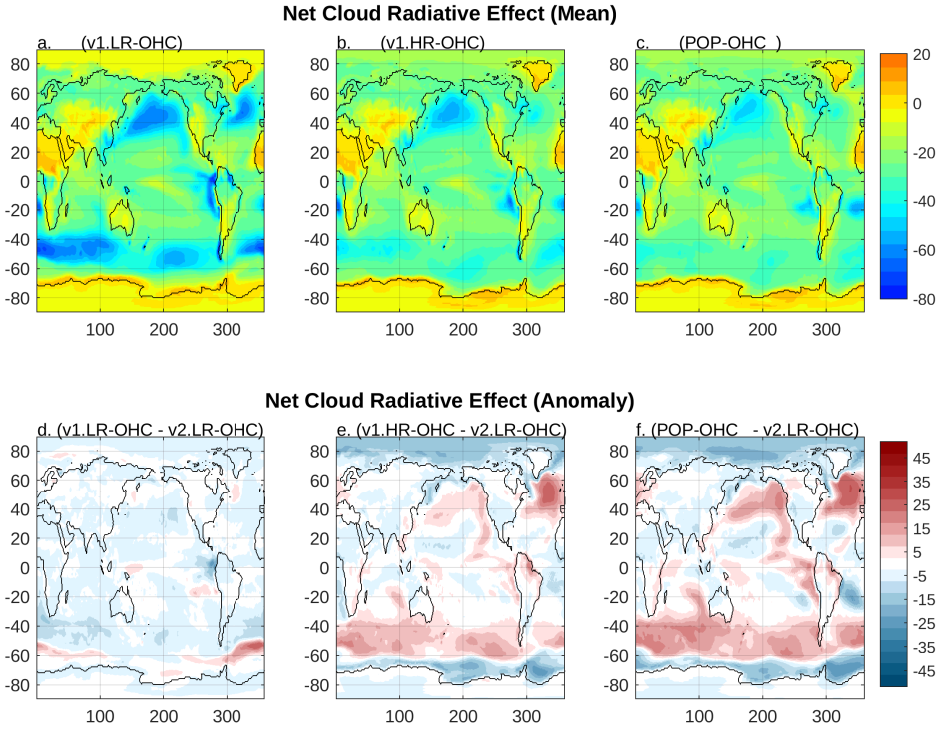

Figure 14. Annual mean net cloud radiative effect (Wm^{-2}) in the SOM.v1.LR-OHC, SOM.v1.HR-OHC, and SOM.P-OHC experiments (a - c), and their difference from the net cloud radiative effect in the SOM.v2.LR-OHC experiment (d - f).

while the cloud radiative effect remained positive. The clear-sky component becomes increasingly negative until it balances the positive cloud radiative effect in equilibrium.

Indeed, there is a global net positive Cloud Radiative Effect (CRE) in high-OHT compared to low-OHT experiments (Figure 14 d-f). The global net positive CRE occurs as a result of a weaker net cloud radiative cooling in high-OHT compared to low-OHT experiments, particularly over the oceans, between 40^o - 60^o in the both hemispheres (compare Figure 14 a - c and e-f). This positive CRE is particularly large over the subpolar North Atlantic where there is also a large prescribed OHC anomaly. However, the impact of the positive CRE over the subpolar Southern Ocean on the global mean is greater, due to the greater ocean area there. The opposite (negative) CRE occurs over the polar regions in both hemispheres, due to a increase in cloud radiative cooling over the polar regions in the high-OHT experiments. However, the positive CRE over the midlatitude regions has a greater impact on the global mean than the negative CRE over the polar regions.

The global net positive CRE occurs mainly through the shortwave rather than the longwave component (compare Figures S5 and S6). Positive shortwave CRE occurs in the subpolar regions during the summer seasons in each hemisphere (Figure S7 and S8), due a decrease in low-level cloud cover in these regions in the High-OHT experiments relative to the low-OHT experiments (Figure 15). Mid-level and high-level cloud fractions are not very different in the two pairs of experiments (Figure S11 and S12). Similar to the spatial pattern of CRE changes, the decrease in low-level cloud cover occurs primarily over the midlatitude regions in both hemispheres, which is particularly large over the subpolar Atlantic and Southern Oceans. Similarly, the negative CRE over the polar regions occurs through an increase in low cloud cover. The decrease in low-level

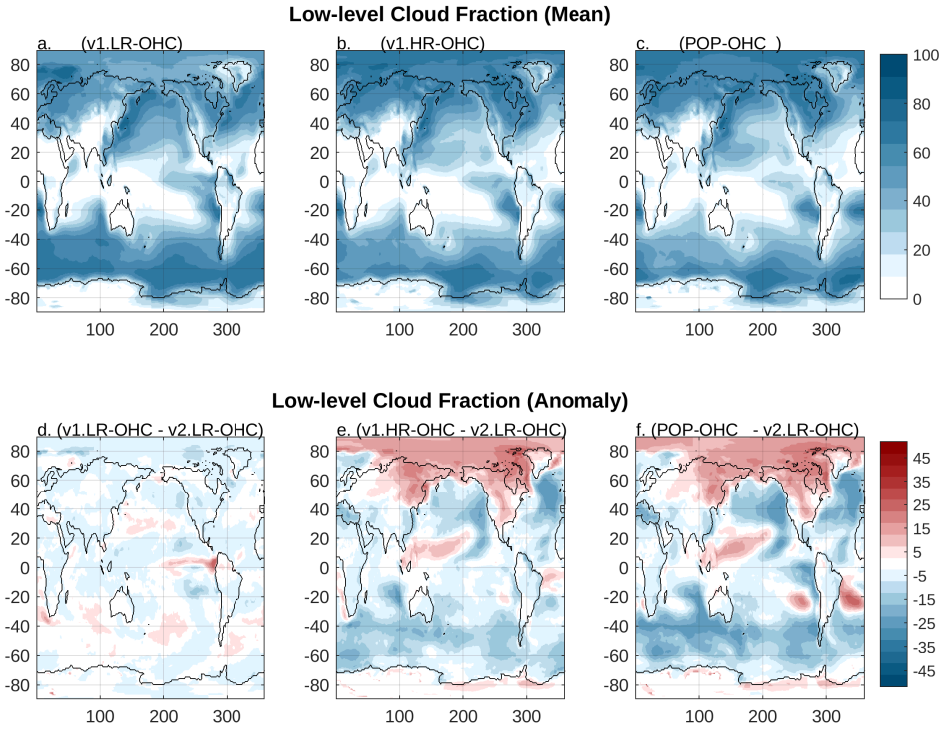

Figure 15. Annual mean low-level cloud fraction (%) in the SOM.v1.LR-OHC, SOM.v1.HR-OHC and SOM.P-OHC (a -c) and their difference from the low cloud fraction in the SOM.v2.LR-OHC experiment(d - f).

clouds over the midlatitudes might also be associated with an increase in precipitation over these regions, particularly over the subpolar Atlantic and Southern hemisphere(Figure 16). There is also a decrease and an increase in precipitation, north and south of the equator respectively, particularly over the Indo-Pacific region.

3.2.1 Climate sensitivity

The fast equilibration time of the SOM makes it particularly useful for the evaluation of the equilibrium climate sensitivity (ECS, Kiehl et al., 2006; Danabasoglu & Gent, 2009; Bitz et al., 2012; Bacmeister et al., 2020; Dunne et al., 2020). The ECS is defined as the equilibrium global surface temperature response to CO_2 doubling. Following Kiehl et al. (2006), we estimate the ECS from equilibrium surface temperature response derived from regression of the first 25 years of the global net TOA heat flux against surface air temperature in the SOM.v2.LR-OHC-4xCO_2 experiment (Figure 17). The regression over this time period is used because it captures the forced response part; after this the simulation is much closer to equilibrium and the temperature changes are largely due to internal variability. By definition, the ECS is the half of the equilibrium temperature response obtained from the 4xCO_2 increase experiment, assuming a linear response to forcing. The ECS can also be estimated as the time-mean value of the surface temperature anomaly during an equilibrium time period in the SOM experiment (Gettelman et al., 2019). The anomalies are calculated with respect to the corresponding time period in the control experiment without CO_2 increase.

An ECS of 4.5°C is obtained from the SOM.v2.LR-OHC-4xCO_2 experiment using the regression method, with an effective radiative forcing (ERF) of 3 Wm^{-2} (Fig-

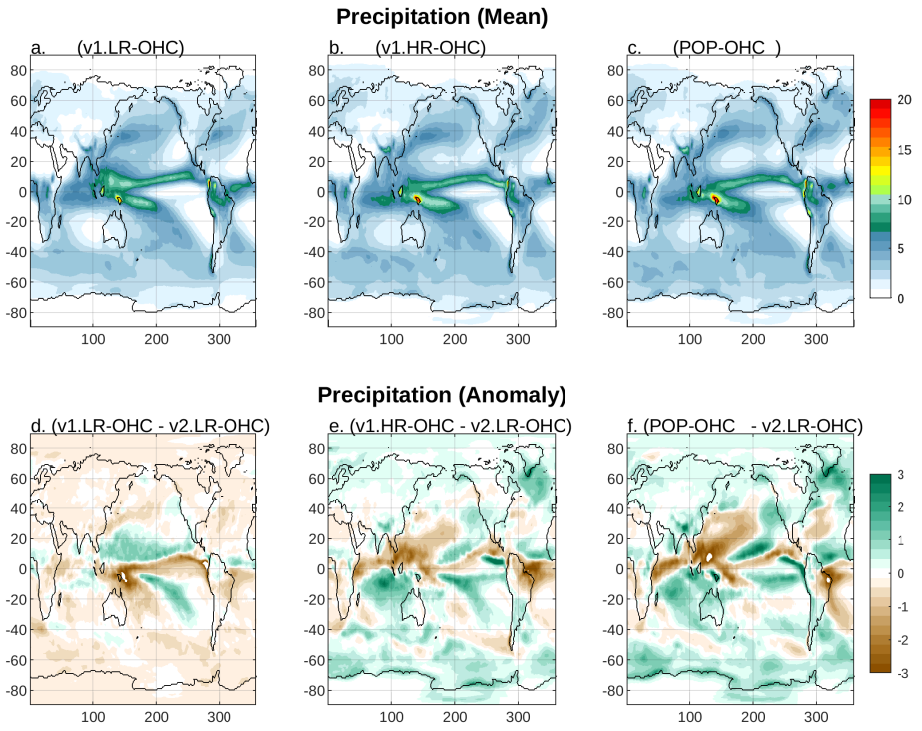

Figure 16. Annual mean precipitation (mm/day) in the SOM.v1.LR-OHC, SOM.v1.HR-OHC, SOM.P-OHC (a - c), and their difference from annual mean precipication in the SOM.v2.LR-OHC experiment (d - f)

ure 17, blue line). Similar ECS and ERF are also obtained from the time-mean values of the anomalies during equilibrated period of years 25 - 50 in the SOM (Figure S14). When compared with the values obtained from the fully coupled v2.LR.piControl experiment using the Gregory method (an extrapolation of the regression over the first 150 years; (Golaz et al., 2022), the ERF derived from the SOM experiment is very similar to estimate obtained from the fully coupled experiment (2.98 Wm^{-2}), while the ECS is different; greater than the fully coupled one (4.0°C) by 0.5°C. The ERF is by definition a property of the atmospheric forcing agent and model (Andrews et al., 2012; Myhre & Coauthors, 2013; Ramaswamy et al., 2018; Andrews et al., 2012), therefore, similar ERF estimates between the SOM and fully coupled experiments is reasonable. Different ECS estimates in the SOM and fully coupled experiment is also reasonable, since SOMs are known to give a higher ECS estimate than their fully coupled analogue (Dunne et al., 2020). The ratio of the ECS estimate in the SOM to the one in the fully coupled is 1.125, which is similar to results from CESM1 and CESM2 (1.23 and 1.22) (Bacmeister et al., 2020) and for most models (Dunne et al., 2020).

Fully coupled models produce lower ECS estimates than SOMs due to atmospheric feedbacks resulting from differences in their surface temperature response patterns (Senior & Mitchell, 2000; Williams et al., 2008; Winton et al., 2013; Garuba et al., 2018). Surface temperature response differences occur between the fully coupled simulations and SOMs, due to the slower Southern Ocean warming rate, and Ocean circulation weakening-induced anomalous surface temperature pattern changes in fully coupled experiments. Ocean circulation weakening due to CO_2 increase in the fully coupled experiments cause changes in the pattern of ocean heat uptake and surface temperature response, which is characterized by the cooler SSTs in the Northern hemisphere, particularly over the sub-

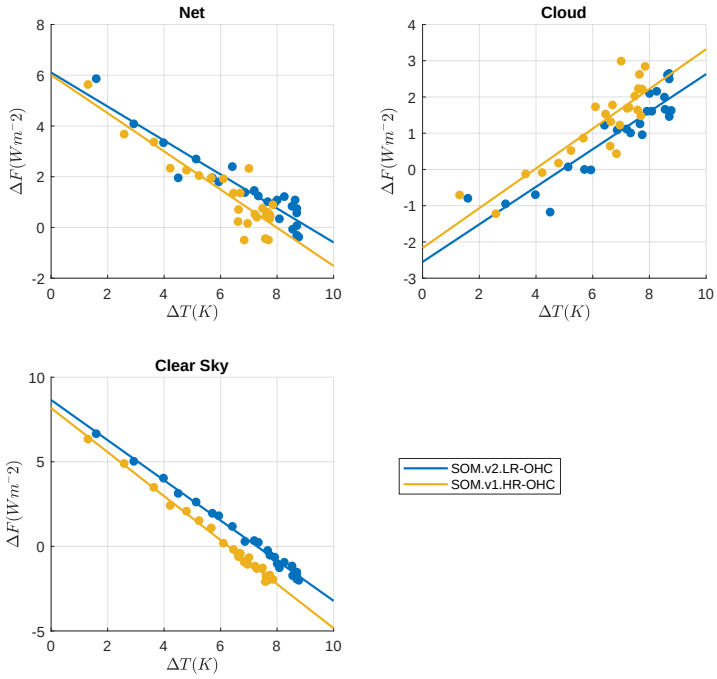

Figure 17. Regression of the annual global TOA heat fluxes against the global surface air temperature in the SOM.v2.LR-OHC-4xCO2 experiments (blue) and SOM.v2.HR-OHC-4xCO2 experiments (yellow). Anomalies are taken with respect to the corresponding years in the SOM.v2LR-OHC and SOM.v1.HR-OHC experiments.

polar Atlantic, and warmer SSTs in the tropical Eastern Pacific (Winton et al., 2013; Garuba et al., 2018). Indeed, SOM SST anomalies are warmer in the subpolar Atlantic and Southern Ocean, but cooler in the tropical Pacific than the fully coupled anomalies (Figure S15). Thse circulation-weakening-induced temperature changes are shown to cause a time-evolving effective climate sensitivity, particularly in the first 150 years (Andrews et al., 2012; Garuba et al., 2018), and ultimately slow down the global surface temperature approach to equilibrium in fully coupled experiments. As a result, the ECS estimate using first 150 years of fully coupled experiments are often underestimated, while the estimates from longer integration of fully coupled experiment become closer to the ECS estimated from the SOM experiment (Williams et al., 2008; Dunne et al., 2020).

The impact of the baseline ocean heat transport strength on the ECS is further examined by comparing the ECS estimates from the SOM.v2.LR-OHC-4xCO_2 experiment and the SOM.v1.HR-OHC-4xCO_2. Recall that the SOM.v2.LR-OHC-4xCO_2 and SOM.v1.HR-OHC-4xCO2 experiments are initialized from the low- and high-OHT (SOM.v2.LR-OHC and SOM.v1-HR-OHC) control experiments respectively which have very different baseline climates. They are also forced with the same OHC prescribed for the respective baseline simulations derived from low- and high-OHT fully coupled simulations. We find that the ECS is also sensitive to the differences in baseline state and prescribed OHCs, while the ERF is not. The ECS obtained from the high-OHT-4xCO_2 experiment (4°C) is 0.5°C cooler than the one from low-OHT-4xCO_2 experiment (4.5°C), while the ERFs are the same in both experiments(3 Wm^{-2}) (Figure 17, yellow line).

ERFs in the SOM.v2.LR-OHC-4xCO_2 and SOM.v1.HR-OHC-4xCO_2 experiments are similar for the same reason the ERFs in SOM.v2.LR.OHC-4xCO_2 and 4xCO2 fully coupled experiments are similar; that is, these experiments share the same atmosphere

model and forcing agents. Similar ERFs were also obtained in the Caldwell et al. (2019) study, using prescribed SSTs from E3SMv1-HR and E3SMv1-LR fully coupled experiments, despite the very different ocean circulation strength. However, different ECS in the low-OHT and high-OHT 4xCO_2 experiments can also be anticipated; ECS are shown to be sensitive to the baseline AMOC strength (Kostov et al., 2014), but this sensitivity is due to a different mechanism from the one described above. The impact of ocean circulation strength on ECS in the low-OHT and high-OHT 4xCO_2 SOM experiments can only occur through a "passive" mechanism which particularly affects the Southern ocean, while its impact on ECS in the 4xCO_2 SOM and its fully coupled analogue also involves the "active one" (Xie & Vallis, 2012; Winton et al., 2013; Marshall et al., 2015; Garuba et al., 2018). As discussed earlier, different ECS estimates obtained from the SOM and fully coupled experiment involve the active weakening of the ocean circulation strength in the fully coupled experiment, which does not occur in the SOM. On the other hand, in the low-OHT/High-OHT 4xCO_2 SOM experiments, the ocean circulation strength is different but remains constant throughout both SOM simulations.

Different ECS estimates between low- and high-OHT-4xCO_2 experiments is caused by differences in their ocean heat transport strengths and initial baseline states. Lower ECS in the high-OHT-4xCO_2 experiment appears to emerge from its greater net climate feedback, which in turn is due to greater its clear-sky feedback (Figure 17, compare blue and yellow line). This different clear-sky feedback occurs as a result of the different baseline sea ice extent and volume in the experiments they are initialized from (Recall Figure 11). Smaller sea ice extent and volume in the high-OHT baseline experiment cause smaller clear sky forcing in the SOM.v1.HR-OHC-4xCO_2 experiment over the polar regions (Figure S16), which is compensated by a negative CRE over these regions in this experiment (Figure S17). The difference in ocean circulation strength also contributes the SST response pattern difference. Southern Ocean heat uptake occurs largely through the passive advection of heat by ocean circulation (Xie & Vallis, 2012; Marshall et al., 2015; Garuba et al., 2018). Stronger/weaker ocean circulation is related to greater/weaker ocean heat uptake and weaker/greater surface temperature response in the Southern Ocean. The Southern ocean surface temperature response is cooler in the SOM.v1.HR-OHC-4xCO_2 than the SOM.v2.LR-OHC-4xCO_2 due to its weaker ocean circulation strength (Figure S18). The warming results in the greater global surface temperature response in the low OHT experiment.

4 Summary and Conclusion

This study introduces and evaluates the slab ocean model (SOM) configuration in E3SMv2. The E3SM-SOM is evaluated by comparing the baseline climate it simulates with that of the fully coupled E3SMv2 preindustrial control simulation. The SOM is able to reproduce the fully coupled simulation climatology very well. Similar to its counterpart within CESM, the SOM is able to produce a very similar (albeit cooler SST) pattern as well as sea ice extent and thicknesses when compared to its fully coupled analogue. The precipitation pattern is also very similar in the SOM and fully coupled experiments. The global averaged biases in the SOM for these variables are all less than 1% of the fully coupled global averages.

The SOM is further employed to study the sensitivity of the E3SMv2 baseline climate to ocean heat transports. A suite of SOM simulations forced with prescribed ocean heat convergences (OHC) that were derived from fully coupled experiments with weaker and stronger ocean heat transport(low- and high-OHT experiments) are compared with the E3SMv2-SOM baseline climate. All the prescribed OHC patterns have zero global averages, such that the climate response to the OHCs arises only from the differences in their patterns. Hence, when compared to the OHC patterns derived from the low-OHT fully coupled experiments, the OHC pattern derived from high-OHT ones, ocean heat convergence strengthening over the subpolar regions, particularly over the subpolar At-

lantic, is compensated by strengthening in heat divergence over the tropical/subtropical regions. Our results shows a large sensitivity of the E3SMv2 baseline climate to the strength of the ocean heat transports, with a global temperature differences of almost 4^oC between the high-OHT and low-OHT SOM experiments. Similar to the OHC pattern driving it, the warm/cold temperature response in the high/low-OHT SOM experiments occur largely over the subpolar regions in both hemispheres with weaker responses in the tropical/subtropical regions. However, the temperature sensitivity to the prescribed OHC is greater in the Southern than Northern hemisphere. The temperature response in the Southern hemisphere is greater than in the Northern hemisphere, even though the OHC forcing is greater in the Northern hemisphere. This large sensitivity to OHC forcing in the Southern hemisphere is also associated with an over-compensation of the prescribed ocean heat transport by atmospheric heat transports there.

The surface temperature sensitivity to OHC variations occur through a positive/negative shortwave cloud radiative effect, which occurs mainly as a result of a decrease/increase in marine low-level clouds over the subpolar regions in response to an increase/decrease in the ocean heat convergence in high-OHT/low-OHT experiments. The decrease/increase in low-level cloud allows more/less shortwave heat flux to be absorbed at the surface, producing a positive feedback on the surface temperature increase/decrease response in the high/low-OHT experiments. Over the polar regions, in the high-OHT experiments, the opposite effect occurs, that is cloud cover increases, resulting in a negative cloud radiative effect. However, the impact of cloud changes over the polar regions is weaker than over the midlatitudes in the global average. The large sensitivity to ocean heat convergence and overcompensation between atmosphere and ocean heat transports in the Southern hemisphere appears to be peculiar to E3SMv2 and possibly indicates that marine clouds are too sensitive to SSTs in this model. Further investigation will be needed to understand the reasons for this large Southern hemisphere sensitivity and overcompensation.

The SOM is further employed to estimate the Equilibrium Climate Sensitivity (ECS) of the model. Similar to general model behaviour, the ECS estimate in the SOM is greater than fully coupled E3SMv2 ECS estimate (4.5°C /4.0°C), while its ERF estimate is similar to that of the fully coupled model (3Wm^{-2} /2.98Wm^{-2}). This behaviour is consistent with what has been found in other models; ECS estimates in fully coupled models, obtained from the extrapolation to equilibrium using the regression of the first 150 years following CO2 increase are found to be generally lower than the one obtained from their respective slab ocean models (Williams et al., 2008; Dunne et al., 2020). This low estimation of ECS from the 150 year-long integration of fully coupled model has been attributed to slower Southern ocean warming rate and time-evolving behavior of climate sensitivity in fully coupled models, which in turn, has been ascribed to the net cooling impact of the ocean circulation weakening response to CO2 increase in the fully coupled models (Senior & Mitchell, 2000; Andrews et al., 2012; Winton et al., 2013; Garuba et al., 2018). A longer integration of the fully coupled E3SMv2 4xCO2 experiment is expected to yield a high ECS estimate that is closer to the slab model estimate, as seen in other models. The ERF on the other hand is similar between the two experiments, which is consistent with fact that ERF is mostly determined by the atmosphere model and forcing agent used.

The SOM ECS estimate is also sensitive to the prescribed ocean heat convergence and the baseline climate the CO2 increase experiment is initiated from. When the ECS estimates in a pair of low-OHT and high-OHT 4xCO_2 SOM experiments are compared, the ECS in the high-OHT (4.0°C) is found to be 0.5°C lower than that of the low-OHT 4xCO2 experiment (4.5°C). Though the net impact of ocean heat transport strength on the ECS here is the same as the impact of ocean heat transport changes on the ECS estimate of the fully coupled experiment described above (i.e they both lower ECS by 0.5°), their mechanisms are different. While the lower ECS in the fully coupled is due to weak-

ening of its ocean circulation, the lower ECS in high-OHT experiment is due to the different baseline state it is initiated from, as well as its greater ocean circulation strength. Greater ocean heat transport strength in the high-OHT experiment produce smaller sea ice extent and volume baseline, which then influence the ECS in high-OHT-4xCO_2 experiment, largely through the clear-Sky feedback component. At the same time, greater ocean circulation strength in the high-OHT experiment cause greater passive heat uptake in the Southern ocean. Passive advection of the anomalies by stronger/weaker ocean circulation is associated stronger/weaker ocean heat uptake and weaker/greater surface temperature response(Xie & Vallis, 2012; Marshall et al., 2015; Garuba et al., 2018). As a result, the high-OHT 4xCO_2 SOM experiment have relatively cooler SSTs in the Southern Ocean than the low-OHT one.

Our results have shown that the E3SMv2-SOM will be a valuable tool for studying the impact of ocean heat transport changes in E3SM. For example, the atmospheric feedbacks responsible for the large sensitivity to changes in ocean heat convergence in the Southern Ocean revealed in our results can be further studied with the SOM for future tuning of the E3SM model. The SOM could also be used to understand the cloud response/feedback to local perturbations to ocean heat convergence, particularly in the polar regions. As in other models, the SOM capability will also be invaluable tool for hierarchical modeling studies.

Acknowledgments

This study was supported by the Regional and Global Model Analysis (RGMA) program area of the Earth and Environmental System Modeling (EESM) program of the U.S. Department of Energy's Office of Science, Biological and Environmental Research (BER), as a contribution to the HiLAT-RASM and WACCEM projects. This study used research computing resources of the National Energy Research Scientific Computing Center (NERSC), a U.S. Department of Energy Office of Science User Facility operated under Contract No. DE-AC02-05CH11231. The Model output for the SOM experiment can be downloaded at http://portal.nersc.gov/archive/home/o/ogaruba/www/E3SM_SlabOverview_data

References

Andrews, T., Gregory, J. M., Webb, M. J., & Taylor, K. E. (2012). Forcing, feedbacks and climate sensitivity in cmip5 coupled atmosphere-ocean climate models. *Geophysical Research Letters*, *39*(9). Retrieved from `https://agupubs.onlinelibrary.wiley.com/doi/abs/10.1029/2012GL051607` doi: https://doi.org/10.1029/2012GL051607

Bacmeister, J. T., Hannay, C., Medeiros, B., Gettelman, A., Neale, R., Fredriksen, H. B., ... Otto-Bliesner, B. (2020). Co2 increase experiments using the cesm: Relationship to climate sensitivity and comparison of cesm1 to cesm2. *Journal of Advances in Modeling Earth Systems*, *12*(11), e2020MS002120. Retrieved from `https://agupubs.onlinelibrary.wiley.com/doi/abs/10.1029/2020MS002120` (e2020MS002120 10.1029/2020MS002120) doi: https://doi.org/10.1029/2020MS002120

Bitz, C. M., Shell, K. M., Gent, P. R., Bailey, D. A., Danabasoglu, G., Armour, K. C., ... Kiehl, J. T. (2012). Climate sensitivity of the community climate system model, version 4. *Journal of Climate*, *25*(9), 3053 - 3070. Retrieved from `https://journals.ametsoc.org/view/journals/clim/25/9/jcli-d-11-00290.1.xml` doi: 10.1175/JCLI-D-11-00290.1

Caldwell, P. M., Mametjanov, A., Tang, Q., Van Roekel, L. P., Golaz, J.-C., Lin, W., ... Zhou, T. (2019). The doe e3sm coupled model version 1: Description and results at high resolution. *Journal of Advances in Modeling Earth Systems*, *11*(12), 4095-4146. Retrieved from `https://agupubs.onlinelibrary.wiley.com/doi/abs/10.1029/2019MS001870` doi:

https://doi.org/10.1029/2019MS001870

Codron, F. (2012). Ekman heat transport for slab oceans. *Climate Dynamics*, *38*, 379–389. Retrieved from https://doi.org/10.1007/s00382-011-1031-3 doi: 10.1007/s00382-011-1031-3

Danabasoglu, G., & Gent, P. R. (2009). Equilibrium climate sensitivity: Is it accurate to use a slab ocean model? *Journal of Climate*, *22*(9), 2494–2499.

Dunne, J. P., Winton, M., Bacmeister, J., Danabasoglu, G., Gettelman, A., Golaz, J.-C., ... Wolfe, J. D. (2020). Comparison of equilibrium climate sensitivity estimates from slab ocean, 150-year, and longer simulations. *Geophysical Research Letters*, *47*(16), e2020GL088852. Retrieved from https://agupubs.onlinelibrary.wiley.com/doi/abs/10.1029/2020GL088852 (e2020GL088852 2020GL088852) doi: https://doi.org/10.1029/2020GL088852

Garuba, O. A., Lu, J., Liu, F., & Singh, H. A. (2018). The active role of the ocean in the temporal evolution of climate sensitivity. *Geophysical Research Letters*, *45*(1), 306–315.

Garuba, O. A., Singh, H. A., Hunke, E., & Rasch, P. J. (2020). Disentangling the coupled atmosphere-ocean-ice interactions driving arctic sea ice response to co 2 increases. *Journal of Advances in Modeling Earth Systems*, *12*(11), e2019MS001902.

Gettelman, A., Hannay, C., Bacmeister, J. T., Neale, R. B., Pendergrass, A. G., Danabasoglu, G., ... Mills, M. J. (2019). High climate sensitivity in the community earth system model version 2 (cesm2). *Geophysical Research Letters*, *46*(14), 8329-8337. Retrieved from https://agupubs.onlinelibrary.wiley.com/doi/abs/10.1029/2019GL083978 doi: https://doi.org/10.1029/2019GL083978

Golaz, J.-C., Caldwell, P. M., Van Roekel, L. P., Petersen, M. R., Tang, Q., Wolfe, J. D., ... others (2019). The doe e3sm coupled model version 1: Overview and evaluation at standard resolution. *Journal of Advances in Modeling Earth Systems*, *11*(7), 2089–2129.

Golaz, J.-C., Van Roekel, L. P., Zheng, X., Roberts, A. F., Wolfe, J. D., Lin, W., ... Bader, D. C. (2022). The doe e3sm model version 2: Overview of the physical model and initial model evaluation. *Journal of Advances in Modeling Earth Systems*, *14*(12), e2022MS003156. Retrieved from https://agupubs.onlinelibrary.wiley.com/doi/abs/10.1029/2022MS003156 (e2022MS003156 2022MS003156) doi: https://doi.org/10.1029/2022MS003156

Hirons, L. C., Klingaman, N. P., & Woolnough, S. J. (2015). Metum-goml1: a near-globally coupled atmosphere–ocean-mixed-layer model. *Geoscientific Model Development*, *8*(2), 363–379. Retrieved from https://gmd.copernicus.org/articles/8/363/2015/ doi: 10.5194/gmd-8-363-2015

Hsu, T.-Y., Primeau, F., & Magnusdottir, G. (2022). A hierarchy of global ocean models coupled to cesm1. *Journal of Advances in Modeling Earth Systems*, *14*(8), e2021MS002979. Retrieved from https://agupubs.onlinelibrary.wiley.com/doi/abs/10.1029/2021MS002979 (e2021MS002979 2021MS002979) doi: https://doi.org/10.1029/2021MS002979

Hurrell, J. W., Holland, M. M., Gent, P. R., Ghan, S., Kay, J. E., Kushner, P. J., ... Marshall, S. (2013). The community earth system model: A framework for collaborative research. *Bulletin of the American Meteorological Society*, *94*(9), 1339 - 1360. Retrieved from https://journals.ametsoc.org/view/journals/bams/94/9/bams-d-12-00121.1.xml doi: https://doi.org/10.1175/BAMS-D-12-00121.1

Jeevanjee, N., Hassanzadeh, P., Hill, S., & Sheshadri, A. (2017). A perspective on climate model hierarchies. *Journal of Advances in Modeling Earth Systems*, *9*(4), 1760-1771. Retrieved from https://agupubs.onlinelibrary.wiley.com/doi/abs/10.1002/2017MS001038 doi: https://doi.org/10.1002/

2017MS001038

Kiehl, J. T., Shields, C. A., Hack, J. J., & Collins, W. D. (2006). The climate sensitivity of the community climate system model version 3 (ccsm3). *Journal of Climate*, *19*(11), 2584 - 2596. Retrieved from https://journals.ametsoc.org/view/journals/clim/19/11/jcli3747.1.xml doi: https://doi.org/10.1175/JCLI3747.1

Knutson, T. (2003). *Fms slab ocean model technical documentation* (Tech. Rep.). Retrieved from https://www.gfdl.noaa.gov/fms-slab-ocean-model-technical-documentation

Kostov, Y., Armour, K. C., & Marshall, J. (2014). Impact of the atlantic meridional overturning circulation on ocean heat storage and transient climate change. *Geophysical Research Letters*, *41*(6), 2108-2116. Retrieved from https://agupubs.onlinelibrary.wiley.com/doi/abs/10.1002/2013GL058998 doi: https://doi.org/10.1002/2013GL058998

Leung, L. R., Bader, D. C., Taylor, M. A., & McCoy, R. B. (2020). An introduction to the e3sm special collection: Goals, science drivers, development, and analysis. *Journal of Advances in Modeling Earth Systems*, *12*(11), e2019MS001821. Retrieved from https://agupubs.onlinelibrary.wiley.com/doi/abs/10.1029/2019MS001821 (e2019MS001821 2019MS001821) doi: https://doi.org/10.1029/2019MS001821

Marshall, J., Scott, J. R., Armour, K. C., Campin, J.-M., Kelley, M., & Romanou, A. (2015). The ocean's role in the transient response of climate to abrupt greenhouse gas forcing. *Climate Dynamics*, *44*, 2287–2299.

McFarlane, N. A., Boer, G., Blanchet, J., & Lazare, M. (1992). The canadian climate centre second-generation general circulation model and its equilibrium climate. *Journal of Climate*, *5*(10), 1013–1044.

Myhre, G., & Coauthors. (2013). Anthropogenic and natural radiative forcing. climate change 2013: The physical science basis, t. f. stocker et al. , 659–740.

Petersen, M. R., Asay-Davis, X. S., Berres, A. S., Chen, Q., Feige, N., Hoffman, M. J., ... others (2019). An evaluation of the ocean and sea ice climate of e3sm using mpas and interannual core-ii forcing. *Journal of Advances in Modeling Earth Systems*, *11*(5), 1438–1458.

Ramaswamy, V., Collins, W., Haywood, J., Lean, J., Mahowald, N., Myhre, G., ... Storelvmo, T. (2018). Radiative forcing of climate: The historical evolution of the radiative forcing concept, the forcing agents and their quantification, and applications. *Meteorological Monographs*, *59*, 14.1 - 14.101. Retrieved from https://journals.ametsoc.org/view/journals/amsm/59/1/amsmonographs-d-19-0001.1.xml doi: https://doi.org/10.1175/AMSMONOGRAPHS-D-19-0001.1

Rasch, P., Xie, S., Ma, P.-L., Lin, W., Wang, H., Tang, Q., ... others (2019). An overview of the atmospheric component of the energy exascale earth system model. *Journal of Advances in Modeling Earth Systems*, *11*(8), 2377–2411.

Ringler, T., Petersen, M., Higdon, R. L., Jacobsen, D., Jones, P. W., & Maltrud, M. (2013). A multi-resolution approach to global ocean modeling. *Ocean Modelling*, *69*, 211-232. Retrieved from https://www.sciencedirect.com/science/article/pii/S1463500313000760 doi: https://doi.org/10.1016/j.ocemod.2013.04.010

Schmidt, G. A., Ruedy, R., Hansen, J. E., Aleinov, I., Bell, N., Bauer, M., ... others (2006). Present-day atmospheric simulations using giss modele: Comparison to in situ, satellite, and reanalysis data. *Journal of Climate*, *19*(2), 153–192.

Senior, C. A., & Mitchell, J. F. B. (2000). The time-dependence of climate sensitivity. *Geophysical Research Letters*, *27*(17), 2685-2688. Retrieved from https://agupubs.onlinelibrary.wiley.com/doi/abs/10.1029/2000GL011373 doi: https://doi.org/10.1029/2000GL011373

Williams, K. D., Ingram, W. J., & Gregory, J. M. (2008). Time variation of ef-

fective climate sensitivity in gcms. *Journal of Climate*, *21*(19), 5076 - 5090. Retrieved from `https://journals.ametsoc.org/view/journals/clim/21/19/2008jcli2371.1.xml` doi: https://doi.org/10.1175/2008JCLI2371.1

Winton, M., Griffies, S. M., Samuels, B. L., Sarmiento, J. L., & Frölicher, T. L. (2013). Connecting changing ocean circulation with changing climate. *Journal of Climate*, *26*(7), 2268 - 2278. Retrieved from `https://journals.ametsoc.org/view/journals/clim/26/7/jcli-d-12-00296.1.xml` doi: https://doi.org/10.1175/JCLI-D-12-00296.1

Xie, P., & Vallis, G. K. (2012). The passive and active nature of ocean heat uptake in idealized climate change experiments. *Climate Dynamics*, *38*, 667–684.